



Open Access This file is licensed under a Creative Commons Attribution 4.0 International License, which permits use, sharing, adaptation, distribution and reproduction in any medium or format, as long as you give appropriate credit to the original author(s) and the source, provide a link to the Creative Commons license, and indicate if changes were made. In the cases where the authors are anonymous, such as is the case for the reports of anonymous peer reviewers, author attribution should be to 'Anonymous Referee' followed by a clear attribution to the source work. The images or other third party material in this file are included in the article's Creative Commons license, unless indicated otherwise in a credit line to the material. If material is not included in the article's Creative Commons license and your intended use is not permitted by statutory regulation or exceeds the permitted use, you will need to obtain permission directly from the copyright holder. To view a copy of this license, visit <http://creativecommons.org/licenses/by/4.0/>.

Reviewers' comments:

Reviewer #1 (Remarks to the Author):

Walsh et al present Mito-SiPE, a new method that enriches for mitochondria before library prep to derive extremely high quality mtDNA for rare heteroplasmy analysis. The method is well justified and the presentation looks technically impressive. The application to the PolG mutator mice is appropriate, and the results clearly indicate that Mito-SiPE can be a valuable tool in the mtDNA analysis toolkit. Overall, the manuscript is in good shape and I commend the authors for their work. I have a few suggestions that may improve the work:

- As far as I can tell, there is no explicit variant calling performed. How do the authors recommend identifying variants from Mito-SiPE data? Sequencing errors, as an example, tend to be non-random where certain regions are more likely than others to yield false heteroplasmy due to Illumina sequencers. I'd recommend a very minimum verifying that the strand concordance (measured by a Fishers test of ref/alt allele and +/- strand) be assessed for variant filtering.

- Previously, when ultra rare sequencing method is developed, a UMI is used to further mitigate PCR bias, perhaps using a consensus collapsing (e.g. see: <https://www.ncbi.nlm.nih.gov/pmc/articles/PMC6723130/>). If the authors could comment on this approach relative to a UMI-based method, this could help presentation.

- Additional analyses of the heteroplasmies, such as annotation in specific genes, complex families, synonymous/ nonsynonymous/ etc., would improve the demonstration of why one should sequence with this approach (i.e. can the authors better justify, using their data, why to use their approach in order to learn new biology).

- It would be of interest to share the distribution of fragment sizes and the percent duplicates (both metrics easily derived from Picard tools) for these libraries or for a subset of them.

- I would encourage the authors to share sequencing data on GEO or a related means as the method is much more likely to be adopted if the data is easily and freely accessible.

Reviewer #2 (Remarks to the Author):

In this manuscript, Walsh et al. describe Mito-SiPE, a method for extracting and enriching Mitochondrial DNA without relying on PCR or probes. The authors showed that most reads in the generated libraries map the mitochondrial genome. Then the authors showed that nuclear-mitochondrial sequences (NUMT) do not contribute significantly to the higher levels of mtDNA mapped reads. Moreover, the authors demonstrated that their technique generates more uniform coverage across the mitochondrial genome than PCR-based methods. Finally, the authors showed that Mito-SiPE significantly reduces false positive variants.

Overall, the technique will interest readers, especially those studying mtDNA mutations. However, it is not clear what is the manuscript's advantage over what Gould et al. demonstrated in 2015 (PCR-Free Enrichment of Mitochondrial DNA from Human Blood and Cell Lines for High Quality Next-Generation DNA Sequencing, Plos One 2015). I have the following concerns that the authors should address before determining whether Mito-SiPE indeed presents an advantage over other techniques:

1- The authors should discuss Gould et al., 2015 and highlight the advantage of Mito-SiPE over that study (if advantages are present).

2- In Figure 2b (top), the authors claim that the lost coverage in the middle part is due to NUMT and

showed that if they map to mtDNA, the coverage is similar to surrounding regions. I recommend demonstrating the pair-wise alignment between that region in mitochondria and the gDNA to substantiate this.

3- Figure 2C showed that gDNA-mapped reads have higher enrichment in Chromosomes 2 and 9. According to the authors, the alignment tool assigned highly repetitive reads to these two chromosomes. The authors used bwa for mapping, which is known to cause this issue. Removing such reads from the bam file before studying the distribution is highly recommended. Use another mapper that can remove multi-mapped read. Alternatively, such reads will have the Tag "XA:Z" or "SA:Z" in the bam file generated by BWA. You can remove reads with such tags using various tools.

4- Supplementary figures 2-5 are not clear. Add a key to the phylogenetic trees to understand the similarity rate.

5- The comparison in terms of mapped reads between IrPCR and Mito-SiPE should be made in percentages to appreciate the difference in efficiency. Mito-SiPE seems to be having significantly lower mapping percentage than IrPCR.

Minor Comment:

What is the full Mito-SiPE? (Sequence-independent PCR-Free Enrichment)? It is nowhere in the main text.

Reviewer #1 (Remarks to the Author):

Walsh et al present Mito-SiPE, a new method that enriches for mitochondria before library prep to derive extremely high quality mtDNA for rare heteroplasmy analysis. The method is well justified and the presentation looks technically impressive. The application to the PolG mutator mice is appropriate, and the results clearly indicate that Mito-SiPE can be a valuable tool in the mtDNA analysis toolkit. Overall, the manuscript is in good shape and I commend the authors for their work. I have a few suggestions that may improve the work:

1) As far as I can tell, there is no explicit variant calling performed. How do the authors recommend identifying variants from Mito-SiPE data? Sequencing errors, as an example, tend to be non-random where certain regions are more likely than others to yield false heteroplasmy due to Illumina sequencers. I'd recommend a very minimum verifying that the strand concordance (measured by a Fishers test of ref/alt allele and +/- strand) be assessed for variant filtering.

This remark is much appreciated as typically a specific variant caller is used to identify rare mutations present in the mitochondrial genome or somatic mutations in tissue/cancer samples. The variant calling in our analysis was carried out using bcftools to count occurrences of reference and alternative alleles after duplication removal. We have altered the methods to make this clearer in the text. During this process both duplication and base quality score were all considered. Whilst we did not specifically filter for strand odds ratio or Fisher's values, our existing variant calling strategy and frequency threshold essentially eliminated any strand biases present. Of 66,738 variants identified across all samples in our study at an alternative allele frequency $\geq 0.2\%$, only 137 of these had a $\ln(\text{Strand Odds Ratio})$ value ≥ 3 . This represents a negligible fraction of total variants observed and omission of these variants had no impact on final analysis. Additionally, we have included a github repository with the code used for alignment and variant calling in the methods section.

We have modified the text in the manuscript at Lines 657-666:

Variant calling and mutation analysis

Variant calling was performed using bcftools v1.9 with 'bcftools mpileup -f -Q 30 --skip-indels reference_fasta bam_file | bcftools call -mv' to identify single nucleotide variants only. Filtering was performed by removing any SNVs that had a QUAL score lower than 30. The code used for alignment and variant calling is available on github (<https://github.com/walshd59/mtDNAhetScripts.git>). Of 66,738 variants identified across all samples in our study at an alternative allele frequency $\geq 0.2\%$, only 137 of these had a $\ln(\text{Strand Odds Ratio})$ value ≥ 3 .

2) Previously, when ultra rare sequencing method is developed, a UMI is used to further mitigate PCR bias, perhaps using a consensus collapsing (e.g. see: <https://www.ncbi.nlm.nih.gov/pmc/articles/PMC6723130/>). If the authors could comment on this approach relative to a UMI-based method, this could help presentation.

The utilisation of UMIs to increase sensitivity of the methodology described is an excellent suggestion and something we anticipate testing in the future. Although our method currently represents a powerful tool for rare-heteroplasmy identification, using a UMI may further enhance its performance. We have included a short comment in the discussion which addresses this point.

Lines 419-427 have been modified in the revised manuscript.

Our methodology is limited by the sequencing error rate that produces false positive heteroplasmy calls. The use of unique molecular identifiers (UMIs) have been shown to reduce the impact of errors and thus increase one's ability to detect rare variants⁴⁶. UMI's are nucleotide 'barcodes' which are ligated to DNA before library preparation. After sequencing, consensus reads are generated from reads that possess the same UMI and thus PCR errors and sequencing errors can be negated. Mito-SiPE, in combination with the use of UMIs, may enable researchers to detect variants at even lower levels than what is documented here.

3) *Additional analyses of the heteroplasmies, such as annotation in specific genes, complex families, synonymous/ nonsynonymous/ etc., would improve the demonstration of why one should sequence with this approach (i.e. can the authors better justify, using their data, why to use their approach in order to learn new biology).*

Thank you for this suggestion. As part of our revised manuscript we have included an analysis of the variants identified in POLG and wild-type mice. Unsurprisingly, Mito-SiPE and IrPCR show very similar results in samples that have high levels of mitochondrial mutation. However, Mito-SiPE negates the impact of PCR errors and artifact-generating NUMT amplification which is evident in the lack of mutations found in C57BL6 mice. In this way, it offers researchers a reliable method of low-frequency variant identification and negates the impact of false positives driven by IrPCR or similar methods. There was no significant difference between Mito-SiPE and IrPCR in terms of location/genes in which mutations were found. Additionally, we calculated the difference in heteroplasmic variants (MAF \geq 0.2%) across the mitochondrial genome between both methodologies (Supplementary Fig. 11, a). This figure shows that false positives occur almost across the whole mitochondrial genome with a marked increase at the locations where IrPCR has reduced coverage. Annotation of these differences did not show a notable difference between low, medium and high impact variants. However more variants were identified in mt-Nd4 and mt-Nd1, which coincides with the IrPCR region of reduced coverage.

The revised manuscript has been modified at Lines: 266-292:

Analysis of the mutation profile observed using both IrPCR and Mito-SiPE showed similar results in *Polg*^{wt/wt} and *Polg*^{D257A/D257A} (Supplementary Fig 10a). *Polg*^{D257A/D257A} mice had higher levels of mutations occurring at 'C' nucleotide positions in the reference genome (light-strand). Interestingly, *Polg*^{wt/wt} had more mutations at the 'A' nucleotide position, indicating that perhaps there is some selection that occurs when mutations are passed from *Polg*^{D257A/wt} to their progeny.

Where IrPCR and Mito-SiPE widely diverged in results was in the mutation spectrum of wildtype C57BL6 mice. Long-range PCR amplification causes an increase in mutations occurring at the 'T' nucleotide position whereas no mutations are identified using Mito-SiPE. This is also in contrast to both groups with a *Polg*^{D257A/wt} background. Due to the large number of mutations that were identified in *Polg*^{D257A/D257A} mouse tissues (1000-7500), high-frequency variants (\geq 10% MAF) were selected for further

sequence analysis (Supplementary Fig 10b; Supplementary data). There was no difference between IrPCR and Mito-SiPE in the mutational spectrum in these high-frequency mutations in terms of profile or proportion of transitions to transversions. Additionally, we observed no difference in the loci/genes in which mutations were identified. The number of mutations found in each gene is now available in Supplementary Data, Table 1. The difference in heteroplasmic variants (MAF \geq 0.2%) across the mitochondrial genome between both methodologies was calculated (Supplementary Fig. 11, a). False positive heteroplasmic variants occur almost across the mitochondrial whole genome with a marked increase at the locations where IrPCR has reduced coverage and decrease in the D-loop region. Annotation of these differences did not show a notable contrast between low, medium and high impact variants. However, more variants were identified in mt-Nd4 and mt-Nd1, which coincides with the IrPCR region of reduced coverage.

The revised manuscript has been modified at Lines 393-399:

Analysis of the variants identified using IrPCR and Mito-SiPE showed reproducible results across Polgwt/wt and PolgD257A/D257A mouse tissues. Mito-SiPE showed improvement in samples that have low to no levels of mitochondrial heteroplasmy. Long-range PCR amplification causes artificially elevated levels of mutation, either through PCR errors or amplification of NUMTs. Mito-SiPE offers researchers a more sensitive approach to detect smaller changes in low-frequency mutations compared to methods that are reliant on PCR.

4) *It would be of interest to share the distribution of fragment sizes and the percent duplicates (both metrics easily derived from Picard tools) for these libraries or for a subset of them.*

Thank you for this suggestion. We have included tables for the library complexity and fragment size metrics as calculated by Picard tools in Supplementary Table 2. These have been calculated for a subset of samples (n = 15) randomly selected from the library.

Library complexity metrics (Picard tools; mean values)		
Optical duplicates (sd)	Percent duplication (sd)	Library size (sd)
702,000 (110,000)	0.52 (0.12)	23,000,000 (4,700,000)

Fragment size metrics (Picard tools; mean values (sd))	
MEDIAN_INSERT_SIZE	346 (18)
MODE_INSERT_SIZE	209 (13)
MEDIAN_ABSOLUTE_DEVIATION	116 (10)
MIN_INSERT_SIZE	3 (2)
MAX_INSERT_SIZE	16297 (6)
MEAN_INSERT_SIZE	365 (18)
STANDARD_DEVIATION	160 (11)
READ_PAIRS	6317968 (1628243)
WIDTH_OF_10_PERCENT	46 (4)
WIDTH_OF_20_PERCENT	92 (8)

WIDTH_OF_30_PERCENT	139 (12)
WIDTH_OF_40_PERCENT	186 (16)
WIDTH_OF_50_PERCENT	234 (21)
WIDTH_OF_60_PERCENT	284 (25)
WIDTH_OF_70_PERCENT	336 (29)
WIDTH_OF_80_PERCENT	394 (32)
WIDTH_OF_90_PERCENT	497 (35)
WIDTH_OF_95_PERCENT	634 (45)
WIDTH_OF_99_PERCENT	1065 (522)

Lines 654-655:

Library complexity and fragment sizes were calculated using Picard tools v 1.4.2 on 15 randomly-selected samples (Supplementary Table 2).

5) *I would encourage the authors to share sequencing data on GEO or a related means as the method is much more likely to be adopted if the data is easily and freely accessible.*

We appreciate this comment and have submitted our sequences to NCBI's SRA. We have uploaded all of the raw reads under the submission reference: SUB12051683 (BioProject: PRJNA881035).

Reviewer #2 (Remarks to the Author):

In this manuscript, Walsh et al. describe Mito-SiPE, a method for extracting and enriching Mitochondrial DNA without relying on PCR or probes. The authors showed that most reads in the generated libraries map the mitochondrial genome. Then the authors showed that nuclear-mitochondrial sequences (NUMT) do not contribute significantly to the higher levels of mtDNA mapped reads. Moreover, the authors demonstrated that their technique generates more uniform coverage across the mitochondrial genome than PCR-based methods. Finally, the authors showed that Mito-SiPE significantly reduces false positive variants.

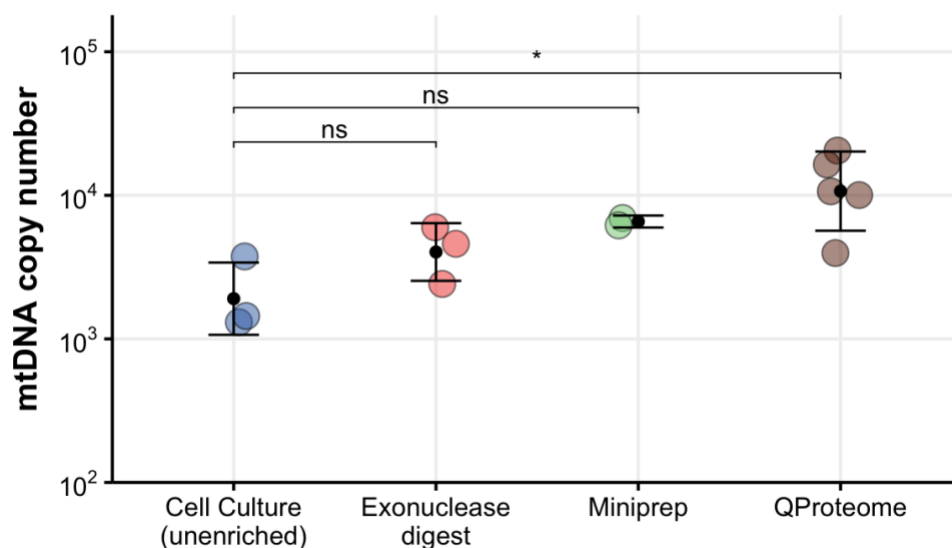
Overall, the technique will interest readers, especially those studying mtDNA mutations. However, it is not clear what is the manuscript's advantage over what Gould et al. demonstrated in 2015 (PCR-Free Enrichment of Mitochondrial DNA from Human Blood and Cell Lines for High Quality Next-Generation DNA Sequencing, Plos One 2015). I have the following concerns that the authors should address before determining whether Mito-SiPE indeed presents an advantage over other techniques:

1- The authors should discuss Gould et al., 2015 and highlight the advantage of Mito-SiPE over that study (if advantages are present).

Thank you for this very insightful suggestion. It was an oversight on our behalf to not include this paper in the introduction and we have corrected that in the revised submission. In unpublished work, we have attempted to use exonuclease digests to enrich mitochondrial DNA. We then quantified the level of enrichment using a qPCR

assay, similarly to Gould et al. 2015. Our qPCR assay results were broadly similar to Gould et al. except we could not achieve efficiency levels as high as their best sample (61.78% of reads aligned to the mitochondrial genome). More importantly, the amount of starting material and/or final DNA concentration post-digest, in our hands, was a substantial limiting factor in the amount of reads that would be achievable and therefore cause significant (1000-to-10,000-fold) reduction in the per-base coverage of the mitochondrial genome. In essence, it may not always be feasible to use this methodology to achieve ultra-high sequencing depth of the mitochondrial genome and thus, rare heteroplasmy analysis. The following is an excerpt from the thesis (from DJW) to be published in the coming months that featured the aforementioned work:

“The exonuclease digest enrichment method results were also comparable to previously published literature (Gould et al. 2015). This group first measured the relative mtDNA levels of blood that was treated with Plasmid-Safe exonuclease using a qPCR assay, similar to the one used in this project. Whilst their qPCR results were comparable to those displayed above, they also performed next-generation sequencing on the same samples and found that a maximum of 61.78% of reads aligned to the mitochondrial genome for one of their samples. This is much higher than our estimation but may be explained by the small total read count achieved during sequencing of said sample (total reads aligned = 16,156) (Gould et al., 2015).”



This figure shows results from said unpublished thesis that compared mtDNA copy number post-enrichment using exonuclease digest, a miniprep kit and Qproteome isolation followed by DNA extraction. These enrichments were carried out on HepG2 cells which may explain some of the discrepancies between our work and Gould et al., who used human blood, the metastatic melanoma cell line COLO 829 and its matched normal lymphoblast line COLO 829BL. We commend Gould et al.'s work as it offers researchers a sequence-independent method that works on cell culture, which is a major difference to what we're reporting here. However, we feel that the final mtDNA read depth and variety of tissues reported in our paper offers a substantial difference/improvement to their method. Finally and importantly, the small number of

aligned reads achieved using Gould et al.'s method makes it unsuitable for low-frequency heteroplasmy quantification at the levels reported in this manuscript. lines 112-117:

A sequence independent method for mitochondrial enrichment carried out on blood and cell culture samples was previously described using an exonuclease digest⁴⁷. Its use on samples with modest amount of starting material offers a unique approach for measuring heteroplasmy in scarce samples such as cultured cells. However, compared to Mito-SiPE, the method yielded a reduced mapping efficiency and sequencing depth on average, limiting its use in low frequency heteroplasmy analysis.

2- In Figure 2b (top), the authors claim that the lost coverage in the middle part is due to NUMT and showed that if they map to mtDNA, the coverage is similar to surrounding regions. I recommend demonstrating the pair-wise alignment between that region in mitochondria and the gDNA to substantiate this.

Thank you for the suggestion. We have included a screenshot from BLAST below. When we query the mitochondrial sequence (MT:7500-11000) against the mouse genome a hit from Chromosome 1 appears and has a 99.94% sequence identity across the full length of the query. In our original text we erroneously claimed 100%, which has now been rectified. The figure below has been included as Supplementary Figure 2.

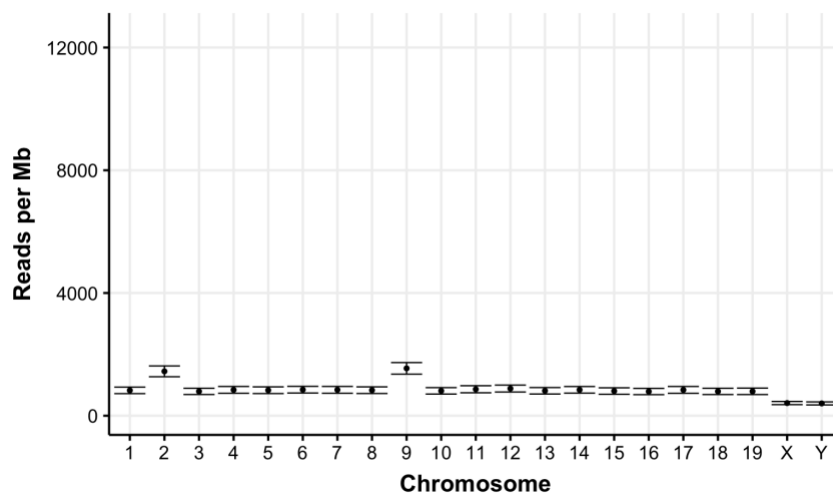
The screenshot shows a BLAST search interface. On the left, the job title is 'MT dna:chromosome chromosome:GRCm39:MT:7500:11000'. The query ID is 'lcl|Query_556235'. The description is 'MT dna:chromosome chromosome:GRCm39:MT:7500:11 ...'. The molecule type is 'dna' and the query length is '3501'. On the right, the 'Filter Results' panel shows the organism as 'Mus musculus' and the percent identity as '99.94%'. Below the filter results, there is a table of sequences producing significant alignments. The table has columns for Description, Scientific Name, Max Score, Total Score, Query Cover, E value, Per. Ident, Acc. Len, and Accession. The first row is selected and shows a hit from 'Mus musculus strain C57BL/6J chromosome 1, GRCm39' with a 99.94% identity.

Description	Scientific Name	Max Score	Total Score	Query Cover	E value	Per. Ident	Acc. Len	Accession
Mus musculus strain C57BL/6J chromosome 1, GRCm39	Mus musculus	6455	7515	100%	0.0	99.94%	195154279	NC_000067.7

We have also modified Lines 181-183 in the revised manuscript. This is due to an NUMT found on chromosome 1 of the reference genome that shares 99.94% sequence identity of its homologous sequence in the mitochondrial genome (Supplementary Fig. 2).

3- Figure 2C showed that gDNA-mapped reads have higher enrichment in Chromosomes 2 and 9. According to the authors, the alignment tool assigned highly repetitive reads to these two chromosomes. The authors used bwa for mapping, which is known to cause this issue. Removing such reads from the bam file before studying the distribution is highly recommended. Use another mapper that can remove multi-mapped read. Alternatively, such reads will have the Tag "XA:Z" or "SA:Z" in the bam file generated by BWA. You can remove reads with such tags using various tools.

Thank you for this suggestion. We agree that if one were to look more closely at the distribution across each chromosome, that removal of these multi-mapped reads would be beneficial. However, our main aim from this demonstration was to show that real mitochondrial reads were being misaligned to Chromosome 1 due to a region with high levels of sequence identity. The repetitive reads that are aligned to Chromosomes 2 and 9 are trivial in this regard. When we removed the reads with the tags "XA:Z" or "SA:Z" in a subset of the samples, the observed elevated coverage was reduced but evident (shown below).



4- *Supplementary figures 2-5 are not clear. Add a key to the phylogenetic trees to understand the similarity rate.*

Thank you for this remark. We have replaced the phylogenetic trees with BLAST results tables to show that the regions on chromosome 2 and 9 have other regions in the mouse genome that share a high level of sequence identity and thus leads to misalignment at these loci.

5- *The comparison in terms of mapped reads between IrPCR and Mito-SiPE should be made in percentages to appreciate the difference in efficiency. Mito-SiPE seems to be having significantly lower mapping percentage than IrPCR.*

Thank you for this observation. We have edited Table 3 to include the percentage of reads aligned to the mitochondrial genome. Your statement is totally correct, IrPCR has a much higher mapping efficiency as has been documented in previous literature (including the Gould et al. paper). Our findings show that even with this lower mapping efficiency, Mito-SiPE increases one's ability to detect low-frequency mutations due to avoiding false-heteroplasmic calls.

Minor

Comment:

What is the full Mito-SiPE? (Sequence-independent PCR-Free Enrichment)? It is nowhere in the main text.

Thank you for this observation, we have defined Mito-SiPE at the end of the introduction.

See Lines 106-107 of the revised manuscript.

We have called this method Mito-SiPE (A sequence-independent, PCR-free mitochondrial DNA enrichment)

1 Mito-SiPE: A sequence-independent, PCR-free mitochondrial DNA enrichment
2 method for ultra-deep sequencing that minimises amplification and alignment artifacts.

3

4 Darren J Walsh^{1,2}, David J Bernard¹, Faith Pangilinan¹, Madison Esposito¹, Denise
5 Harold², Anne Parle-McDermott², Lawrence C Brody¹ (corresponding author).

6

7 1 - Gene and Environment Interaction Section, National Human Genome Research
8 Institute, NIH, Bethesda, MD, USA.

9 2 – School of Biotechnology, Dublin City University, Dublin, Ireland.

10

11 **Abstract**

12 **Background**

13 The analysis of somatic variation in the mitochondrial genome requires deep
14 sequencing of the mitochondrial genome. This is ordinarily achieved by selective
15 enrichment methods, such as PCR amplification or probe hybridization. These
16 methods can introduce bias and are prone to contamination by nuclear-mitochondrial
17 sequences (NUMTs), elements that can introduce artefacts into heteroplasmy
18 analysis.

19 **Results**

20 Here, we demonstrate a method to obtain ultra-deep (>80,000X) sequencing coverage
21 of the mitochondrial genome by selectively purifying the organelle with differential
22 centrifugation and alkaline lysis of seven different mouse tissues. This method yields
23 a preparation of highly enriched mtDNA and avoids the pitfalls inherent in the widely
24 employed sequence dependent methods. This methodology avoids false-
25 heteroplasmy calls that occur when long-range PCR amplification is used for mtDNA
26 enrichment.

27 **Discussion**

28 Mitochondrial DNA from the un-adapted version of this method did not undergo
29 quantification or short-read sequencing when it was initially reported. Here, we have
30 described a modified version of the protocol and have quantified the increased level
31 of mitochondrial DNA post-enrichment in 7 different mouse tissues. This method will
32 enable researchers to identify changes in low frequency heteroplasmy without
33 introducing PCR biases or NUMT contamination that are falsely identified as
34 heteroplasmy when long-range PCR is used.

35 **Abbreviations**

36 NUMT – Nuclear mitochondrial sequences

37 mtDNA – Mitochondrial DNA

38 POLG – Polymerase gamma

39 UMI – unique molecular identifier

40

41 **Introduction**

42

43 Decades of research have established a link between mitochondrial DNA variation and
44 human health. Recent advances in DNA sequencing technologies have led to an
45 increased ability to interrogate the mitochondrial genome for low-frequency mutations
46 associated with various disease states. Mitochondrial DNA mutations have been
47 associated with ageing¹ and a myriad of disease phenotypes². Disorders caused by
48 inherited and acquired mitochondrial DNA variants affect ~1 in 4,300 of the
49 population³. These variants were initially thought to solely originate from matrilineal
50 inheritance of mitochondrial DNA molecules, however more recent studies have
51 shown that somatic mutations also occur in mtDNA over time in a tissue-specific
52 manner⁴⁻⁶. There are hundreds-to-thousands of mitochondrial DNA molecules in every
53 human cell. This number is dependent on the tissue, cell type and energy state of the
54 mitochondria⁷. The fluctuating, multi-copy nature of mitochondrial DNA means that
55 mutations can be present at any frequency within a cell, unlike the diploid nuclear
56 genome. The presence and frequency of mitochondrial DNA mutations is referred to
57 as mitochondrial heteroplasmy.

58

59 Mitochondrial heteroplasmy has been increasingly investigated as a contributor to
60 human disease. To date, it has been linked to various diseases including
61 cardiomyopathy, hypertension, epilepsy, Parkinsons disease and optic neuropathy⁸⁻
62 ¹². Elevated heteroplasmy levels have also been linked to tumor aggressiveness and
63 poor cancer prognoses^{13,14}. These studies demonstrate that mitochondrial
64 heteroplasmy analysis could help to identify unknown molecular mechanisms that
65 drive some disease states. Additionally, evidence suggests that mitochondrial DNA
66 heteroplasmy could be used as a potential target for diagnosis/prognosis of particular
67 conditions and even perhaps as a therapeutic target¹⁵. Given these findings, it is
68 important that mitochondrial heteroplasmy, particularly low frequency heteroplasmy,

69 can be identified and quantified as a part of disease-related studies. Such
70 investigations require high to ultra-high sequencing coverage (>1000X - >10,000X) of
71 the mitochondrial genome in order to reliably quantitate low frequency heteroplasmy
72 with a high degree of sensitivity and specificity. Currently, this is typically achieved by
73 using probe hybridisation or long-range polymerase chain reaction (PCR) to enrich
74 mitochondrial DNA.

75

76 Probe Hybridisation¹⁶ uses complementary probes that bind mitochondrial sequences
77 to separate mtDNA from nuclear DNA. Another approach is long-range PCR¹⁷ which
78 amplifies the mitochondrial genome, typically in two, overlapping fragments. Both
79 probe hybridization and long-range PCR amplification require complementary binding
80 of probes/primers to enrich mtDNA from whole DNA extracts. Widespread use of these
81 methodologies in many heteroplasmy studies is due to their ease, amenability to high-
82 throughput processes and efficacy of producing mtDNA appropriate for ultra-deep
83 sequencing^{4,5,18,19}. These sequence-dependent methods are imperfect. Probes and
84 primers designed to match reference alleles may select against rare heteroplasmic
85 variants that are of interest. Additionally, PCR amplification is known to introduce
86 errors that may appear as false positive heteroplasmic variants. Arguably, the most
87 problematic issue for these techniques is the contamination of nuclear-mitochondrial
88 elements (NUMTs)²⁰.

89

90 NUMTs are nuclear sequences that share high levels of sequence identity with
91 mtDNA. They had arisen from the somatic translocation of mitochondrial DNA into the
92 nuclear genome. The number, size and sequence of NUMTs varies within species²¹,
93 including between human populations and individuals²². The entire mitochondrial
94 genome is represented in the human nuclear genome²². As a result of this, it is
95 extremely difficult to design primers or hybridization probes that will selectively enrich
96 mitochondrial DNA without also enriching NUMT sequences. Multiple studies have
97 found that NUMT contamination was present in mtDNA sequencing data that used
98 either probe hybridisation or PCR amplification to enrich mtDNA^{23–26}. Most notably,
99 NUMT contamination is thought to explain the apparent paternal inheritance of
100 mitochondrial DNA in humans that was reported in PNAS in 2018^{27–30}. The difficulty
101 posed by deciphering NUMT contamination from true mitochondrial DNA may require
102 the usage of a sequence-independent method for mitochondrial enrichment.

103

104 Here, we have adapted a previously described³¹ sequence-independent and PCR-free
105 technique which relies on differential centrifugation and alkaline lysis to separate
106 mitochondria from other tissue/cellular debris. We have called this method Mito-SiPE
107 (a sequence-independent, PCR-free mitochondrial DNA enrichment). We provide
108 evidence that this method can be effectively used to isolate mitochondrial DNA from
109 different tissues for subsequent mtDNA sequencing, achieving ultra-deep coverage of
110 the mitochondrial genome when combined with an appropriate NGS data pipeline.

111

112 A sequence independent method for mitochondrial enrichment carried out on blood
113 and cell culture samples was previously described using an exonuclease digest³². Its
114 use on samples with modest amount of starting material offers a unique approach for
115 measuring heteroplasmy in scarce samples such as cultured cells. However,
116 compared to Mito-SiPE, the method yielded a reduced mapping efficiency and
117 sequencing depth on average, limiting its use in low frequency heteroplasmy analysis.

118

119 *Polg* mutator mice are used as positive controls to compare Mito-SiPE with long-range
120 PCR amplification enrichment of mtDNA. These mice lack the ability to ‘proof-read’
121 their mitochondrial DNA and as a result, gather single nucleotide mutations at a much
122 higher frequency than their wild-type counterparts³³. We propose that this method can
123 be applied to a range of species to allow researchers to reliably investigate
124 mitochondrial heteroplasmy and expand our current knowledge of the contribution of
125 somatic mitochondrial mutations to human ageing and disease. This methodology
126 negates the impact of NUMT contamination and PCR error introduction when
127 assessing heteroplasmy and is therefore more sensitive and accurate than long-range
128 PCR amplification.

129

130 **Results**

131

132 This technique for enriching mtDNA for sequencing is rooted in classic cell biology and
133 biochemistry methods for subcellular fractionation. It utilizes a combination of
134 differential centrifugation and alkaline lysis to separate the mitochondria from nuclear
135 and cytoplasmic cellular components. The preparation is then used to purify
136 mitochondrial DNA with minimal contamination from nuclear DNA (Fig. 1a). To test

137 this method, we used it on seven different mouse tissues; brain, heart, lung, kidney,
138 liver, spleen and muscle. Mitochondrial copy number was assessed *via* quantitative
139 polymerase chain reaction (qPCR) in enriched samples from the seven tissues and
140 compared to unenriched, whole DNA extracts (Fig. 1b). qPCR was used to calculate
141 the ratio of mitochondrial DNA to nuclear DNA, which provides an estimate of the
142 average mtDNA copy number per cell. A significant increase (100-1,000 fold, $P <$
143 0.0005) in mitochondrial DNA copy number was observed in samples that underwent
144 enrichment. This effect was present across the 7 tissues of interest (Fig. 1c).

145

146 The performance of this technique to produce pure, high-quality mtDNA for next-
147 generation DNA sequencing was assessed by applying the method to 163 samples
148 across seven different mouse tissues. These samples were then sequenced across
149 four lanes of the Illumina NovaSeq platform. After quality control, alignment and
150 removal of duplicates, the number of mitochondrial, nuclear and unmapped reads
151 were assessed for each sample (Fig. 1d, Table 1). Of the mapped reads, an average
152 of $75\% \pm 20\%$ were mapped to the mitochondrial genome and $25\% \pm 20\%$ to the nuclear
153 genome. Unmappable reads made up $0.26 \pm 0.63\%$ (Table 2). The level of nuclear
154 contamination in samples originating from brain, heart, kidney and liver was extremely
155 low with higher levels found in lung, muscle and spleen (Fig. 1e).

156

157 Two alignment strategies were used to assess the coverage of the mitochondrial
158 genome and the distribution of nuclear contamination (Fig. 2a). The first method
159 aligned filtered reads to the whole genome and then isolated mitochondrial-aligned
160 reads. The second method aligned all the reads to the mitochondrial genome first,
161 then mapped any remaining unaligned reads to the nuclear genome. Coverage across
162 the mitochondrial genome and distribution of nuclear contamination were assessed
163 after duplicate removal. Average coverage across the mitochondrial genome
164 exceeded 50,000X at each base pair and was dependent on tissue of origin (Fig 2b).
165 Lung, muscle and spleen had lower levels of coverage due to the higher levels of reads
166 mapped to nuclear DNA in these samples. Mapping to the whole genome caused a
167 loss in coverage between nucleotide positions 7,500-11,000 (Fig. 2b, top). This dip in
168 coverage was not observed when reads were first aligned to the mitochondrial genome
169 using the second alignment strategy (Fig. 2b, bottom). The latter method did not lead
170 to an overall increase in sequencing coverage across the rest of the mitochondrial

171 genome, indicating that nuclear reads were not misaligned to the mitochondrial
172 genome when this method was used.

173

174 As this mtDNA enrichment method is sequence-independent, any reads that originate
175 from nuclear DNA should have been randomly distributed throughout the whole
176 genome. To test this hypothesis, the distribution of nuclear contamination was
177 assessed using both alignment strategies (Fig 2c). When reads were aligned to the
178 whole genome, nuclear contamination appeared to be evenly distributed across the
179 nuclear genome as expected, except for chromosome 1 (Fig 2c, top). Aligning the
180 reads to the mitochondrial genome first did not produce this same anomaly (Fig 2c,
181 bottom and Supplementary Fig. 1). **This is due to an NUMT found on chromosome 1
182 of the reference genome that shares 99.94% sequence identity of its homologous
183 sequence in the mitochondrial genome (Supplementary Fig. 2).** As a result, the
184 alignment tool (bwa) mapped ~50% of reads originating from this region to the
185 mitochondrial genome and ~50% incorrectly, to the homologous NUMT on
186 chromosome 1 when reads were mapped to the whole genome. This artefact was
187 eliminated when reads were mapped to the mitochondrial genome first. Chromosomes
188 2 and 9 also had slightly elevated levels of mapped reads when compared to the rest
189 of the genome. This effect was produced by both alignment strategies. However,
190 further investigation showed that this was caused by the alignment of highly repetitive
191 reads from across the genome to the same loci on chromosomes 2 and 9
192 (Supplementary Fig. 3,4 and Supplementary Fig. 5,6, respectively). Mapping to the
193 mitochondrial genome first appeared to be more effective at mapping true
194 mitochondrial reads correctly, without increasing levels of spurious alignments. This
195 alignment methodology was used to assess heteroplasmy levels in the tissues of
196 *Polg*^{D257A/D257A} and *Polg*^{wt/wt} mice.

197

198 There was an average of 7.15×10^7 reads produced per sample across all studied
199 groups (Table 3; n=48). A higher average number of reads was observed in the IrPCR
200 amplification samples (7.22 and 7.19×10^7 , *Polg*^{D257A/D257A} (n=12) and *Polg*^{wt/wt} (n=12),
201 respectively) compared to the mtDNA prep samples (7.15 and 7.02×10^7
202 *Polg*^{D257A/D257A} and *Polg*^{wt/wt}, respectively). The proportion of reads mapped to the
203 mitochondrial genome was also higher in the IrPCR amplification samples than the
204 mtDNA preparation samples (Table 3). The average coverage across the

205 mitochondrial genome was higher in the long-range PCR amplification samples
206 (Average depth 137,000X compared to mtDNA prep average of 123,000X). However,
207 these samples had a loss in coverage towards the end of the two overlapping
208 fragments (Fig 3a, left). The mitochondrial DNA prep samples, broadly, had uniform
209 coverage across the whole mitochondrial genome compared to the IrPCR samples.
210 *Polg*^{D257A/D257A} samples displayed minor region-specific fluctuations in coverage (Fig
211 3a, right). This effect was not observed in the long-range PCR amplification assay (Fig
212 3a, middle).

213

214 Three metrics were measured to assess heteroplasmy levels in *Polg*^{D257A/D257A} and
215 *Polg*^{wt/wt} tissues: the number of heteroplasmic sites, the average alternative allele
216 frequency (average heteroplasmy) and cumulative heteroplasmic burden. These three
217 metrics have previously been reported in the literature^{14,34–38}. The number of
218 heteroplasmic sites is the number of nucleotide positions at which an alternative allele
219 was identified above the threshold frequency (0.2%) in a sample. Alternative allelic
220 calls caused by sequencing error are present below this frequency and are
221 indistinguishable from low-frequency heteroplasmy. Average heteroplasmy is the
222 mean frequency of all variants observed in a sample above the threshold frequency.
223 Finally, cumulative heteroplasmic burden is the sum of all variant frequencies that
224 were identified above the threshold frequency in a sample.

225

226 More heteroplasmic sites were observed in the *Polg*^{D257A/D257A} mice than wild-type, in
227 brain, liver and kidney (Fig 3b, top). No difference was observed between
228 *Polg*^{D257A/D257A} males and females, however there was a significant difference between
229 sexes of *Polg*^{wt/wt} (Fig 3b, top, left panels vs right panels). There were significantly
230 fewer heteroplasmic sites found in mtDNA preps of both male and female *Polg*^{wt/wt} as
231 well as *Polg*^{D257A/D257A} males compared to IrPCR enrichment. This effect was not
232 statistically significant in female *Polg*^{D257A/D257A} tissues. The difference between
233 enrichment assays was larger in *Polg*^{D257A/D257A} samples than in *Polg*^{wt/wt}
234 (Supplementary Fig. 7). When examining cumulative heteroplasmic burden, similar
235 overall results were observed (Fig 3b, middle). Lower burden was detected in mtDNA
236 prep enriched samples compared to IrPCR in the same 3 of 4 comparisons. Average
237 heteroplasmy, however, displayed contrasting results (Figure 3b, bottom).
238 *Polg*^{D257A/D257A} mice had lower average heteroplasmy levels than *Polg*^{wt/wt} mice. In

239 *Polg*^{D257A/D257A} mice, the mean alternative allele frequency was significantly lower in
240 mtDNA preps than in IrPCR enrichment. *Polg*^{wt/wt} mice appeared to have higher
241 average heteroplasmy levels, which were elevated in mtDNA preps compared to
242 IrPCR amplification enrichment.

243

244 *Polg*^{wt/wt} mice have a baseline of mitochondrial DNA mutation much higher than that
245 of true wild-type C57BL6 mice (169 ± 29.4 and 0.06 ± 0.24 heteroplasmic sites,
246 respectively). This is because heterozygous female breeders have an intermediate
247 phenotype. Long-range PCR amplification enrichment was performed on total DNA
248 extracted from brain, kidney and liver of two wild-type C57BL6/J males. These
249 enrichments were compared to mtDNA preparation of 6 control C57BL6 males. These
250 mice were age-matched. There was a significant and substantial increase in the
251 number of heteroplasmic sites, cumulative heteroplasmic burden and average
252 heteroplasmy in the IrPCR samples compared to samples that underwent mtDNA
253 preparation (Figure 3c).

254

255 Mitochondrial DNA prep enrichment was performed on 7 tissues of *Polg*^{wt/wt} and
256 *Polg*^{D257A/D257A} mice. Mutant mice displayed significantly higher levels of mitochondrial
257 DNA mutation than wild-type across all tissues (Supplementary Fig. 8). Kidney, liver,
258 colon, heart and lung had a similar number of heteroplasmic sites in *Polg*^{D257A/D257A}
259 mice with higher levels observed in spleen and lower levels found in brain
260 (Supplementary Fig. 9a). Colon and spleen had higher levels of average heteroplasmy
261 than the other five tissues in *Polg*^{D257A/D257A} mice (Supplementary Fig. 9b). Cumulative
262 heteroplasmic burden was higher in *Polg*^{D257A/D257A} colon and spleen tissues and lower
263 in brain than in heart, kidney, liver and lung (Supplementary Fig. 9c). There was no
264 significant difference between the tissues of *Polg*^{wt/wt} mice across any of the three
265 heteroplasmy metrics that were assessed.

266

267 Analysis of the mutation profile observed using both IrPCR and Mito-SiPE showed
268 similar results in *Polg*^{wt/wt} and *Polg*^{D257A/D257A} (Supplementary Fig 10a). *Polg*^{D257A/D257A}
269 mice had higher levels of mutations occurring at 'C' nucleotide positions in the
270 reference genome (light-strand). Interestingly, *Polg*^{wt/wt} had more mutations at the 'A'
271 nucleotide position, indicating that perhaps there is some selection that occurs when
272 mutations are passed from *Polg*^{D257A/wt} to their progeny.

273

274 Where IrPCR and Mito-SiPE widely diverged in results was in the mutation spectrum
275 of wildtype C57BL6 mice. Long-range PCR amplification causes an increase in
276 mutations occurring at the 'T' nucleotide position whereas no mutations are identified
277 using Mito-SiPE. This is also in contrast to both groups with a *Polg*^{D257A/wt} background.
278 Due to the large number of mutations that were identified in *Polg*^{D257A/D257A} mouse
279 tissues (1000-7500), high-frequency variants ($\geq 10\%$ MAF) were selected for further
280 sequence analysis (Supplementary Fig 10b; Supplementary data). There was no
281 difference between IrPCR and Mito-SiPE in the mutational spectrum in these high-
282 frequency mutations in terms of profile or proportion of transitions to transversions.
283 Additionally, we observed no difference in the loci/genes in which mutations were
284 identified. The number of mutations found in each gene is now available in
285 Supplementary Data, Table 1. The difference in heteroplasmic variants (MAF $\geq 0.2\%$)
286 across the mitochondrial genome between both methodologies was calculated
287 (Supplementary Fig. 11, a). False positive heteroplasmic variants occur almost across
288 the mitochondrial whole genome with a marked increase at the locations where IrPCR
289 has reduced coverage and decrease in the D-loop region. Annotation of these
290 differences did not show a notable contrast between low, medium and high impact
291 variants. However, more variants were identified in mt-Nd4 and mt-Nd1, which
292 coincides with the IrPCR region of reduced coverage.

293

294 Discussion

295

296 In this study we have demonstrated that a sequence-independent technique for
297 mitochondrial DNA enrichment is highly effective and can produce ultra-deep
298 sequencing coverage required for heteroplasmy analysis. We conclude that this
299 methodology works most effectively with brain, heart, liver and kidney samples,
300 however sufficient results can also be obtained in samples originating from lung,
301 muscle and spleen. The cause of the disparity between tissues is unknown, however,
302 we hypothesise that it may be related to the amount of starting material, the
303 mechanical properties of the tissues and mitochondrial copy number before
304 enrichment. There are three main advantages of this method over the current
305 standard: 1) It does not require complementary binding of reference probes/primers to
306 mitochondrial DNA, 2) PCR amplification is not required and therefore generates no

307 polymerase errors during enrichment and 3) Any nuclear contamination present is
308 randomly distributed across the nuclear genome and therefore does not result in
309 NUMT enrichment.

310

311 The sequencing depth achieved using this methodology exceeds that of many
312 heteroplasmy studies to-date, even in the tissues where enrichment was less
313 effective^{5,19,39,40}. High coverage of the mitochondrial genome allows for a more
314 sensitive assessment of low frequency mutations and changes in heteroplasmy
315 frequency. The number of reads (average 22.4 million per sample, Table 1) produced
316 through sequencing in this study could be reduced by up-to 5-fold and would still be
317 sufficient to achieve coverage levels in-line with previous studies (typically less than
318 10,000X). This would reduce the sequencing costs, increase throughput and enable
319 the study of mitochondrial heteroplasmy across many samples by taking advantage of
320 high-throughput sequencing. Our results also suggest that sufficient sequencing
321 coverage could be achieved even with lower-capacity sequencing platforms.

322

323 An alternative bioinformatics pipeline is required when this technique is utilized.
324 Typically, it is advised to align all sequencing data to the whole reference genome
325 before isolating mitochondrial reads to avoid spurious alignment of nuclear reads to
326 the mitochondrial genome⁴¹. However, due to the lack of sequence-specific
327 enrichment when using this technique, a different approach is optimal. When reads
328 are aligned to the whole reference genome first, mitochondrial reads are incorrectly
329 aligned to homologous regions in the nuclear genome, most prominently, chromosome
330 1. This effect in this study, it should be noted, is specific to the mouse reference
331 genome; however, future studies may assess whether the same effect is observed in
332 human alignments or indeed in other species. As we demonstrate here, mapping
333 reads to the mitochondrial genome first did not appear to lead to an increase in
334 spurious alignment of nuclear reads to the mitochondrial genome and produced
335 uniform sequencing coverage.

336

337 Nuclear-mitochondrial sequences have been identified as an important source of
338 artefacts in heteroplasmy analysis. By employing sequence-independent enrichment
339 of mitochondrial DNA we find that any nuclear contamination present in the resultant
340 sequence data is randomly distributed across the nuclear genome. It is pertinent to

341 note, however, that although NUMT contamination is not enriched for in this study, it
342 does not mean that NUMT contamination is entirely absent. This is an important point
343 as the number and size of all NUMTs have not been fully elucidated for most species
344 and varies within species, even between individuals. The effect of NUMT
345 contamination when using this technique will be minimised in the tissues that contain
346 less nuclear contamination e.g., brain, heart, kidney and liver.

347

348 Mitochondrial DNA heteroplasmy has been assessed in different ways across a
349 number of studies. Number of heteroplasmic sites, average alternative allele
350 frequency and cumulative heteroplasmic burden are all metrics that have been
351 considered^{14,34–38}. The number of heteroplasmic sites and cumulative heteroplasmic
352 burden was higher in *Polg*^{D257A/D257A} mouse tissues than in that of *Polg*^{wt/wt}, using both
353 IrPCR amplification and mtDNA preparation methods. These findings are in-line with
354 previous studies, however the number of mutations detected appear to be higher in
355 the data presented here. This may be due to high levels of coverage achieved and a
356 lower minimum threshold of alternative allele frequency (0.2%) utilised in this study.
357 Interestingly, *Polg*^{wt/wt} mice displayed lower average alternative allele frequencies than
358 *Polg*^{D257A/D257A}. This effect, at first observation, is in stark contrast to what has been
359 recorded previously and is not what one would expect from the literature. However,
360 the high number of low-frequency heteroplasmies identified in *Polg*^{D257A/D257A} tissues
361 have caused a decrease in the overall average heteroplasmy levels (average
362 alternative allele frequency) compared to *Polg*^{wt/wt} as a result of the high sequencing
363 depth achieved across all samples. This result highlights the importance of looking at
364 multiple measures of heteroplasmy to get an accurate assessment of the levels of
365 mitochondrial DNA mutation that are present in a sample.

366

367 Mitochondrial DNA enriched *via* IrPCR amplification had a higher number of
368 heteroplasmic sites and cumulative heteroplasmic burden than DNA enriched using
369 the mtDNA prep method. This difference was larger in *Polg*^{D257A/D257A} mice than in
370 *Polg*^{wt/wt}. There are two likely explanations for this observation. The first, that rounds
371 of PCR amplification cause PCR errors that are subsequently identified as
372 mitochondrial heteroplasmy, although a high-fidelity polymerase is used to negate this
373 impact as much as possible. The second mechanism is that NUMT regions in the
374 nuclear genome are being co-amplified and thus are mistaken for heteroplasmic,

375 mitochondrial reads. If the first mechanism was the leading cause, it is unexpected
376 that the difference would be higher in *Polg*^{D257A/D257A} tissues than in *Polg*^{wt/wt}, as the
377 error rate of the polymerase used for amplification should remain constant. Co-
378 amplification of NUMT regions, however, could be affected by changes in mtDNA copy
379 number – a feature that has previously been identified in *Polg* mutator mice^{42–44}.
380 Changes in mtDNA copy number may directly affect the amount of mispriming of
381 NUMTs that occurs during IrPCR. Whilst the results described here cannot rule out
382 either mechanism, this evidence leans to co-amplification of NUMT regions as a more
383 likely/influential candidate mechanism for what is thought to be false positive
384 heteroplasmic variants identified in PCR amplified samples. The metric of average
385 alternative allele frequency did not display this same pattern but as explained
386 previously, it is influenced by the presence of many apparent, low-frequency
387 heteroplasmies that are identified when using IrPCR amplification at these sequencing
388 depths and heteroplasmy threshold. This effect was even more dramatic when IrPCR
389 was compared to mtDNA enrichment prep of C57BL6 wild-type tissues. This is largely
390 due to the high baseline of mutation that is present in *Polg*^{wt/wt} due to the intermediate
391 phenotype of female breeder mice.

392

393 Analysis of the variants identified using IrPCR and Mito-SiPE showed reproducible
394 results across *Polg*^{wt/wt} and *Polg*^{D257A/D257A} mouse tissues. Mito-SiPE showed much
395 improvement in samples that have low-no levels of mitochondrial heteroplasmy. Long-
396 range PCR amplification causes artificially elevated levels of mutation, either through
397 PCR errors or amplification of NUMTs. Mito-SiPE offers researchers a more sensitive
398 approach to detect smaller changes in low-frequency mutations than methods reliant
399 on PCR.

400

401 Finally, a tissue-specific effect on the levels of heteroplasmy was observed using the
402 mtDNA prep method in *Polg*^{D257A/D257A} mice. Spleen and colon samples had higher
403 levels of heteroplasmy compared to heart, kidney, liver and lung, whereas, brain
404 samples had lower levels. Heart, kidney, liver and lung were indistinguishable from
405 one-another. This is an interesting finding, as previous studies have identified strong,
406 tissue-specific effects of mitochondrial heteroplasmy in more tissues than what is
407 reported here^{37,45,46}. It is possible that enrichment methods used in previous studies
408 have identified false heteroplasmic variants due to NUMT co-enrichment, and thus the

409 differences observed are due to mtDNA copy number changes, rather than true
410 mtDNA mutations. It is also possible, however, that the levels of coverage and low
411 thresholds used in this study have led to this difference.

412

413 **One** limitation of this methodology is that it requires the availability of tissue for
414 enrichment and as such it may not be feasible for archived DNA samples. DNA purified
415 from intact cells and tissues using standard methods are predominantly nuclear DNA.
416 These preparations and already existing NGS data are not compatible with this
417 method. However, with the explosion of interest in mtDNA and increasing levels of
418 heteroplasmy-focused research, this method will provide an important tool for future
419 explorations of mtDNA variation and its role in aging and disease. **Our methodology is**
420 **limited by the sequencing error rate that produces false positive heteroplasmy calls.**
421 **The use of unique molecular identifiers (UMIs) have been shown to reduce the impact**
422 **of errors and thus increase one's ability to detect rare variants^{47,48}. UMI's are**
423 **nucleotide 'barcodes' which are ligated to DNA before library preparation. After**
424 **sequencing, consensus reads are generated from reads that possess the same UMI**
425 **and thus PCR errors and sequencing errors can be negated. Mito-SiPE, in**
426 **combination with the use of UMIs, may enable researchers to detect variants at even**
427 **lower levels than what is documented here.**

428

429 In conclusion, differential centrifugation and alkaline lysis may be used to enrich
430 mitochondrial DNA free from PCR amplification or probe hybridization. Avoiding
431 sequence-dependent techniques greatly reduces the effect of NUMT contamination, a
432 problem which has been identified in previous studies^{23,24,28,30}. This technique, in
433 addition to a modified bioinformatics pipeline, can be applied to different tissues and
434 achieves ultradeep sequencing coverage. It provides a straightforward and robust
435 workflow to assess heteroplasmy in mitochondrial DNA. This technique outperforms
436 long-range PCR amplification and negates the potential impact of PCR errors and
437 NUMT contamination on heteroplasmy analysis.

438

439 **Legends**

440 Figure 1. PCR-free enrichment of mitochondrial DNA using differential centrifugation
441 and alkaline lysis.

442

443 **a**, Overview of sequence-independent and PCR-free mitochondrial DNA enrichment
444 workflow. Homogenisation and differential centrifugation are used to enrich
445 mitochondria. Alkaline lysis is then used to isolate mitochondrial DNA from any
446 remaining nuclear DNA. **b**, Relative quantification of mtDNA copy number from seven
447 different mouse tissues that underwent enrichment. Mitochondrial DNA to nuclear
448 DNA ratio (mtDNA:nuDNA) was assessed *via* qPCR. $P < 0.0005$ Wilcoxon signed rank
449 test. Log scaled. **c**, The mtDNA:nuDNA ratio across seven different tissues which
450 underwent enrichment. (n=2) for each tissue (brain, heart, lungs, liver, kidney, spleen
451 and muscle). **d**, The distribution of nuclear, mitochondrial and unmappable reads
452 generated in each sample displayed as boxplots (n=163). **e**, The distribution of total
453 and mapped reads across seven mouse tissues after mtDNA enrichment; Brain
454 (n=26), Heart (n=26), Kidney (n=25), Liver (n=21), Lungs (n=26), Muscle (n=12) and
455 Spleen (n=27).

456

457 Figure 2. Alignment of sequencing data to whole-genome reference leads to
458 misalignment of mitochondrial reads. Contaminating nuclear reads are randomly
459 distributed across the whole genome.

460

461 **a**, Overview of two methods for mapping sequencing data; *via* whole genome mapping
462 or mapping exclusively to the mitochondrial genome followed by mapping of unaligned
463 reads to the nuclear genome. **b**, Top, sequencing coverage across the mitochondrial
464 genome of seven mouse tissues when reads are mapped to the whole reference
465 genome. A 'hole' in coverage is observed between nucleotide positions 7,500-11,000.
466 Bottom, sequencing coverage across the mitochondrial genome of seven mouse
467 tissues when reads are mapped exclusively to the mitochondrial reference genome.
468 **c**, Top, the box plots represent the distribution of reads mapped per megabase of DNA
469 to each chromosome when reads are aligned to the whole reference genome. Bottom,
470 the box plots represent the distribution of reads mapped per megabase of DNA to each
471 chromosome when reads are aligned exclusively to the mitochondrial genome. The
472 points represent the average reads per Mb mapped for each tissue.

473

474 Figure 3. Mitochondrial DNA preparations outperform long-range PCR amplification
475 and reduce the impact of PCR errors and NUMT contamination on mitochondrial
476 heteroplasmy.

477

478 **a**, Left, read coverage across the mitochondrial genome after sequencing and
479 alignment for each enrichment method. The average sequencing depth was higher in
480 the IrPCR (blue) samples than those enriched using the mtDNA preparation method
481 (orange). There was a significant reduction of coverage towards the end of each
482 amplicon fragment in the IrPCR samples. This reduction was not observed in the
483 mtDNA prep samples. Right, differences in the average sequencing depth between
484 $Polg^{wt/wt}$ (green) and $Polg^{D257A/D257A}$ (red) using mtDNA prep (left) and IrPCR (right)
485 methodologies. The sequencing depth of $Polg^{D257A/D257A}$ tissues enriched using the
486 mtDNA prep method showed a region-specific variation in coverage, however the
487 average coverage remained comparable between both genotypes. This region-
488 specific pattern was not observed in samples enriched using IrPCR. The standard
489 deviations were larger in IrPCR enriched samples, with one fragment showing larger
490 differences than the other. This was likely due to PCR efficiency or variations due to
491 attempts to mix both fragments in equimolar ratios.

492

493 **b**, top, the number of heteroplasmic sites (alternative allele frequency $\geq 0.2\%$) that
494 were identified in each sample. $Polg^{D257A}$ tissues had more heteroplasmic sites than
495 $Polg^{wt}$. There were significantly less heteroplasmic sites observed in mtDNA prep
496 samples of $Polg^{wt}$ males and females, and in $Polg^{D257A}$ males than in IrPCR enriched
497 samples. This effect was not significant in the $Polg^{D257A}$ females. Middle, The
498 cumulative heteroplasmic burden identified across all samples using both
499 methodologies. Cumulative heteroplasmic burden displayed a similar pattern to the
500 number of heteroplasmic sites; significantly lower levels were detected in $Polg^{wt}$ males
501 and females and in $Polg^{D257A}$ males. The difference was not significant in $Polg^{D257A}$
502 females. Bottom, 7 The average alternative allele frequency (average heteroplasmy)
503 observed across all samples using both enrichment methodologies. Average
504 alternative allele frequency displayed a different pattern of results compared to the
505 previous two heteroplasmy metrics. $Polg^{D257A}$ tissues had lower mean alternative allele
506 frequencies than $Polg^{wt}$. Significantly higher mean alternative allele frequencies were
507 observed in IrPCR tissues from both male and female $Polg^{D257A}$ mice. Conversely,
508 $Polg^{wt}$ samples enriched using the mtDNA prep methodology had higher mean
509 alternative allele frequency than those enriched via IrPCR. Tissues are highlighted by

510 colour, each line represents the same tissue that was enriched using both
511 methodologies. Statistical comparisons between IrPCR and mtDNA prep were
512 performed using a Wilcoxon signed-rank test. There were 24 IrPCR samples and 24
513 mtDNA prep samples (*Polg*^{wt} n=24, *Polg*^{D257A} n=24). Two samples for each tissue, sex
514 and genotype were analysed.

515

516 **c**, Heteroplasmy levels of C57BL6 wild-type mice using both IrPCR and mtDNA prep
517 enrichment methods. Mitochondrial DNA from C57BL6 tissues that were enriched
518 using IrPCR had substantially higher levels of heteroplasmy across the three assessed
519 metrics; top, number of heteroplasmic sites, middle, cumulative heteroplasmic burden
520 and bottom, average heteroplasmy. Unlike the *Polg* mutator mouse comparisons,
521 these enrichments were not performed on the same tissues however the mice were
522 the same sex and age at sacrifice. Statistical comparisons between IrPCR and mtDNA
523 prep were performed using a paired Student's T-test. There were six samples in the
524 IrPCR group and twelve samples in the mtDNA prep group.

525

526 **Supplementary figure 1. The distribution of nuclear contamination across the genome**
527 **shown as boxplots for each tissue.**

528

529 **Supplementary figure 2. Sequence alignment results between NUMT on chromosome**
530 **1 and its homologous region on chromosome 1 which shows 99.94% sequence**
531 **identity.**

532

533 **Supplementary figure 3. Integrated genome viewer (IGV) image of high-coverage**
534 **region on chromosome 2. This image shows the region that reads have aligned to on**
535 **chromosome 2 due to its sequence similarity with other regions in the genome.**

536

537 **Supplementary figure 4. BLAST results table that shows the high level of sequence**
538 **identity between the repetitive region on chromosome 2 and similar regions on other**
539 **chromosomes in the mouse genome.**

540

541 **Supplementary figure 5. Integrated genome viewer (IGV) image of high-coverage**
542 **region on chromosome 9. This image shows the region that reads have aligned to on**
543 **chromosome 9 due to its sequence similarity with other regions in the genome.**

544

545 Supplementary figure 6. BLAST results table that shows the high level of sequence
546 identity between the repetitive region on chromosome 9 and similar regions on other
547 chromosomes in the mouse genome.

548

549 Supplementary figure 7. The difference in number of heteroplasmic sites found
550 between IrPCR and mtDNA preparations in *Polg*^{D257A/D257A} and *Polg*^{wt/wt} tissues shown
551 as boxplots.

552

553 Supplementary figure 8. The number of heteroplasmic sites identified in each tissue
554 of *Polg*^{D257A/D257A} and *Polg*^{wt/wt} mice (n=4). Wilcoxon rank-sum test.

555

556 Supplementary figure 9. The tissue-specific pattern of mutation across *Polg*^{D257A/D257A}
557 and *Polg*^{wt/wt} mice. a, Kidney, liver, colon, heart and lung had a similar number of
558 heteroplasmic sites in *Polg*^{D257A/D257A} mice with higher levels observed in spleen and
559 lower levels found in brain. b, Colon and spleen had higher levels of average
560 heteroplasmy than the other five tissues in *Polg*^{D257A/D257A} mice. c, Cumulative
561 heteroplasmic burden was higher in *Polg*^{D257A/D257A} colon and spleen tissues and lower
562 in brain than in heart, kidney, liver and lung. Wilcoxon rank-sum test with kidney acting
563 as comparator for each statistical test.

564

565 Supplementary figure 10. Characterisation of variants that were found across all
566 samples using both IrPCR and Mito-SiPE. a, Long-range PCR amplification displayed
567 similar results to Mito-SiPE in terms of proportion of mutations which occurred at each
568 nucleotide in the mitochondrial genome. *Polg*^{D257A/D257A} mice had a much larger
569 number of mutations compared to *Polg*^{wt/wt} and C57Bl6 wild-type mice. There was a
570 significant difference in the mutations found in C57Bl6 between IrPCR and Mito-SiPE.
571 b, Mutations that were present at a frequency $\geq 10\%$ heteroplasmy showed similar
572 mutational profiles between IrPCR and Mito-SiPE. Although the Ts/Tv ratios appeared
573 to be slightly different, this was not statistically significant (Chi-squared, $p=0.43$).

574

575 Supplementary figure 11. a, The difference in number of heteroplasmic sites identified
576 using both methods plotted by location. The x axis represents the location in the
577 mitochondrial genome (grouped as 100bp regions) and the y axis represents the

578 difference in the number of heteroplasmic sites found in all samples using lrPCR and
579 Mito-SiPE. Long range PCR amplification has more variants identified across the
580 whole genome with a marked increase at locations where sequencing depth is
581 reduced. The red line represents the average difference between the methods across
582 the whole mitochondrial genome. b, Annotation of the variants using snpEff. Variants
583 were annotated and characterised by their predicted effect. There was no obvious
584 pattern between the difference of high, medium and low impact variants; however,
585 more variants were identified using lrPCR in mt-Nd1 and mt-Nd4 genes. These genes
586 are located in a region that has lower sequencing depth using lrPCR than Mito-SiPE.
587

588 Table 1. The number of mitochondrial, nuclear and unmapped reads per tissue.

Number of reads (millions)

<i>Tissue</i>	Mitochondrial (sd)	Nuclear (sd)	Unmapped (sd)
<i>Brain</i>	20.027 (3.285)	2.575 (2.729)	0.073 (0.178)
<i>Heart</i>	19.636 (2.166)	2.188 (1.481)	0.042 (0.099)
<i>Kidney</i>	17.428 (4.224)	4.783 (4.344)	0.012 (0.021)
<i>Liver</i>	18.931 (4.071)	3.291 (3.774)	0.081 (0.171)
<i>Lungs</i>	12.206 (2.938)	9.860 (3.137)	0.057 (0.134)
<i>Muscle</i>	13.146 (3.467)	9.093 (3.589)	0.156 (0.252)
<i>Spleen</i>	13.813 (3.827)	9.301 (4.368)	0.037 (0.072)
All Tissues	16.641 (4.586)	5.700 (4.660)	0.057 (0.139)

589

590

591 Table 2. The percentage of reads aligned to the mitochondrial genome, nuclear
592 genome and unmappable reads.

Percentage of total reads

<i>Tissue</i>	Mitochondrial (sd)	Nuclear (sd)	Unmapped (sd)
<i>Brain</i>	88.64 (11.09)	11.02 (11.20)	0.34 (0.85)
<i>Heart</i>	89.93 (6.19)	9.87 (6.23)	0.21 (0.50)
<i>Kidney</i>	78.68 (18.60)	21.26 (18.63)	0.06 (0.10)
<i>Liver</i>	85.14 (15.36)	14.52 (15.43)	0.33 (0.63)
<i>Lungs</i>	55.30 (13.21)	44.44 (13.30)	0.26 (0.60)
<i>Muscle</i>	58.90 (15.02)	40.39 (14.98)	0.71 (1.17)
<i>Spleen</i>	60.15 (16.53)	39.69 (16.54)	0.16 (0.32)
All Tissues	74.64 (19.76)	25.10 (19.78)	0.26 (0.63)

593

594

595 Table 3. The average total number of reads, mapped reads and sequencing depth for
 596 each methodology and genotype.

Assay type	Genotype	Total reads		Mapped reads		Coverage	
		Average (10 ⁷)	SD	Average (10 ⁷)	SD	Average (10 ⁵)	SD
IrPCR amplification	<i>Polg</i> ^{D257A}	7.22	0.561	7.19 (99.5%)	0.50	1.39	0.417
mtDNA prep	<i>Polg</i> ^{D257A}	7.15	0.848	3.98 (55.7%)	1.86	1.22	0.245
IrPCR amplification	<i>Polg</i> ^{wt}	7.19	0.687	7.08 (98.5%)	0.693	1.36	0.411
mtDNA prep	<i>Polg</i> ^{wt}	7.02	0.687	4.53 (64.5%)	1.79	1.25	0.126

597

598 Methods

599 Breeding and tissue harvesting

600 All animal protocols were reviewed and approved by the National Human Genome
 601 Research Institute (NHGRI) Animal Care and Use Committee prior to animal
 602 experiments. Mice were housed in shoe box cages and fed ProLab RMH 1800 diet
 603 (PMI Nutrition International) containing 50 µg vitamin B12/kg of diet and 3.3 mg folic
 604 acid/kg of diet. Breeding mice were fed Picolab Mouse Diet 20, containing 51 µg
 605 vitamin B12/kg diet and 2.9 mg folic acid/kg of diet. Heterozygous *Polg*^{wt/D257A} males
 606 and *Polg*^{wt/D257A} females were mated. Homozygous mutant and wild-type progeny
 607 were aged to 6 months at which point they were sacrificed. There were 4 *Polg*^{wt/wt} mice
 608 (2 male, 2 female) and 4 *Polg*^{D257A/D257A} mice (2 male, 2 female) used in the *Polg*
 609 experiments. Brain, heart, lung, liver, spleen, kidney and muscle tissue was isolated
 610 and mitochondrial DNA enrichment was performed on all tissues

611

612 Tissue homogenisation

613 Harvested tissue was placed in a homogenization tube with 10X volume per gram of
 614 fresh homogenization buffer i.e. 5 ml buffer for 500 mg tissue. Tissues were

615 homogenised until no discernible whole tissue was present. The homogenate was
616 then transferred to 1.5 ml microcentrifuge tubes and spun at 1000 g for 1 minute at
617 4°C. The supernatant was transferred to a new microcentrifuge tube and spun at 12000
618 g for 10 minutes at 4°C to pellet mitochondria. The mitochondrial pellet was
619 resuspended with 100 µl of resuspension buffer for storage or for immediate DNA
620 extraction.

621

622 **Mitochondrial DNA isolation**

623 The mitochondria resuspension was added to 200 µl alkaline lysis buffer, vortexed,
624 and placed on ice for 5 minutes. Potassium Acetate Buffer (150 µl) was then added
625 and the mixture was vortexed slowly and placed on ice for 5 minutes. The mixture was
626 centrifuged at 12,000 g for 5 minutes at 4°C to pellet proteins and the supernatant was
627 decanted to a new tube. RNase (1 µg) was added to the mixture and left at room
628 temperature for 15 minutes. Phenol-chloroform (500 µl) was added to each tube,
629 inverted and placed on a shaker/rotator for 20 minutes. Afterwards, centrifugation at
630 12000 g for 2 minutes at room temperature was carried out. The aqueous (top) layer
631 was decanted to a new tube (approx. 450 µl from this phase was retrieved) and 40 µl
632 sodium acetate, 1 µl glycogen (20 mg/ml) and 1200 µl 100% EtOH were added. The
633 mixture was inverted and mixed well then left on dry ice for 60 minutes. The mixture
634 underwent centrifugation at 12,000 g and the supernatant was removed. The pellet
635 was finally washed twice using 70% ethanol, air-dried, and resuspended in a low-TE
636 buffer for sequencing or regular TE buffer for (q)PCR.

637

638 **Library preparation and next generation DNA sequencing**

639 Libraries were generated from approximately 50 ng genomic DNA using the Accel-
640 NGS 2S Plus DNA Library Kit (Swift Biosciences) using 5 cycles of PCR to minimize
641 PCR bias. The DNA samples were sheared by sonication (Covaris Inc., Woburn, MA)
642 to a mean of 300 bp. Libraries were tagged with unique dual index DNA barcodes to
643 allow pooling of libraries and minimize the impact of barcode hopping. Libraries were
644 pooled for sequencing on the NovaSeq 6000 (Illumina) to obtain at least 7.6 million
645 151-base read pairs per individual library. Sequencing data was processed using RTA
646 version 3.4.4.

647

648 **Data processing and alignment**

649 Fastq files were aligned to the mouse reference genome, GRCm38, using bwa mem
650 using the default parameters⁴⁹. Picard tools were used to add read groups, and to
651 mark and remove duplicates⁵⁰. Samtools was used to calculate the coverage across
652 the nuclear and mitochondrial genome for each sample. Finally, R (v3.5.0) and ggplot2
653 (v3.3.0) were used for statistical analysis and subsequent visualisation of graphs^{51,52}.
654 **Library complexity and fragment sizes were calculated using Picard tools v 1.4.2 on**
655 **15 randomly-selected samples (Supplementary table 2).**

656

657 **Variant calling and mutation analysis**

658 **Variant calling was performed using bcftools v1.9 with 'bcftools mpileup -f -Q 30 -skip-**
659 **indels reference_fasta bam_file | bcftools call -mv' to identify single nucleotide variants**
660 **only. Filtering was performed by removing any SNVs that had a QUAL score lower**
661 **than 20. The code used for alignment and variant calling is available on github**
662 **(<https://github.com/walshd59/mtDNAhetScripts.git>). Of 66,738 variants identified**
663 **across all samples in our study at an alternative allele frequency $\geq 0.2\%$, only 137 of**
664 **these had a $\ln(\text{Strand Odds Ratio})$ value ≥ 3 . Analysis of the mutation spectrum and**
665 **further characterisation/annotation of heteroplasmic variants was performed using**
666 **SnEff (v 5.1)⁵³.**

667

668 **Quantification of mtDNA copy number**

669 Mitochondrial DNA copy number was assessed via qPCR targeting both mt-16S and
670 nuclear-encoded hexokinase (HK), similarly as previously described⁵⁴. Briefly, 2.5 μl
671 LightCycler® 480 SYBR Green I Master (Roche, Molecular Systems, Inc, Germany),
672 2 μl of DNA (20 ng/ μl) and 0.5 μl primer mix were added in triplicate to a 384-well plate
673 and the reactions were carried out by the QuanStudio 6 Flex (Applied Biosystems,
674 Foster City, CA, USA). The conditions were as follows: 95°C for 5 min, 45 cycles of
675 95°C for 10 s, 60°C for 10 s and 72°C for 20 s. A melting curve was performed using
676 95°C for 5 s, 66°C for 1 min and gradual increase to 97°C. Mitochondrial DNA copy
677 number was assessed using the following formula: $2 \times 2^{\Delta\text{Ct}}$ where $\Delta\text{Ct} = \text{Ct}(\text{mtDNA}$
678 $\text{gene}) - \text{Ct}(\text{nDNA gene})$.

679

680 **Long-range PCR enrichment of mtDNA**

681 This technique was used to amplify human and mouse mitochondrial DNA in two
682 fragments from a whole DNA extract. DNA was quantified *via* Nanodrop (Methods
683 2.2.7) unless otherwise stated. Each PCR reaction consisted of Q5 High-fidelity
684 Polymerase (0.02 U/ μ l), 5X Q5 reaction buffer (1X), 10mM dNTPs (300 μ M), 5 μ M
685 Forward and Reverse primers (0.25 μ M, Table 2.3; human, Table 2.4; mouse).
686 Template DNA (100 ng) was added to each reaction except for the no-template control
687 (NTC) but an equivalent volume of molecular biology grade water was added instead.
688 The temperature cycles were as follows: 1 x 30 s denature 98°C, 25 x 10 s denature
689 98°C, 30 s annealing 66°C, 4 minutes 30 s elongation 72°C, 1 x 10 minutes elongation
690 72°C on a thermocycler. Both fragments were quantified using qubit and mixed in
691 equimolar ratios.

692

693 **Statistics and reproducibility**

694 All statistical analyses included in this paper were carried out in R (version 4.1.1) and
695 the software package rstatix (version 0.7.0). Sample sizes are described within each
696 experimental figure.

697

698 **Solutions**

699 Homogenization Buffer:	0.25 M Sucrose, 10 mM EDTA, 30 mM Tris-HCl, 700 pH=7.5.
701 Resuspension Buffer:	10 mM Tris, 0.15 M NaCl, 10 mM EDTA, pH=8.0.
702 Alkaline Lysis Buffer:	0.18 N NaOH, 1% SDS (Prepare fresh).
703 Potassium Acetate Buffer:	3M potassium, 5M acetate.
704 Low TE buffer:	10 mM Tris-HCl, 0.1 mM EDTA, pH=8.0.

Ethics approval and consent to participate

Not applicable

Consent for publication

Not applicable

Availability of data and materials

All sequencing data and associated metadata is available on SRA (PRJNA881035).

Competing interests

The authors declare that they have no competing interests

Funding

This work was funded by Wellcome Trust, National Human Genome Research Institute and NIH Intramural Sequencing Centre.

Author Contributions

DW, ME and DB performed the sample collections and enrichment. DW and DH performed bioinformatics and subsequent analysis. DW, DB, FP, DH, APMcD and LB prepared manuscript. All authors read and approved the final manuscript.

References

1. Kauppila, T. E. S., Kauppila, J. H. K. & Larsson, N.-G. Mammalian Mitochondria and Aging: An Update. *Cell Metab.* **25**, 57–71 (2017).
2. Stewart, J. B. & Chinnery, P. F. The dynamics of mitochondrial DNA heteroplasmy: implications for human health and disease. *Nat. Rev. Genet.* **16**, 530–542 (2015).
3. Gorman, G. S. *et al.* Prevalence of nuclear and mitochondrial DNA mutations related to adult mitochondrial disease. *Ann. Neurol.* **77**, 753–759 (2015).

4. Li, M., Schröder, R., Ni, S., Madea, B. & Stoneking, M. Extensive tissue-related and allele-related mtDNA heteroplasmy suggests positive selection for somatic mutations. *Proc. Natl. Acad. Sci.* **112**, 2491–2496 (2015).
5. Ma, H. *et al.* Germline and somatic mtDNA mutations in mouse aging. *PLoS ONE* **13**, (2018).
6. Zhang, R., Wang, Y., Ye, K., Picard, M. & Gu, Z. Independent impacts of aging on mitochondrial DNA quantity and quality in humans. *BMC Genomics* **18**, (2017).
7. Kelly, R. D. W., Mahmud, A., McKenzie, M., Trounce, I. A. & St John, J. C. Mitochondrial DNA copy number is regulated in a tissue specific manner by DNA methylation of the nuclear-encoded DNA polymerase gamma A. *Nucleic Acids Res.* **40**, 10124–10138 (2012).
8. Zhang, D. *et al.* Mitochondrial DNA mutations activate the mitochondrial apoptotic pathway and cause dilated cardiomyopathy. *Cardiovasc. Res.* **57**, 147–157 (2003).
9. Golob, M. J. *et al.* Mitochondria DNA mutations cause sex-dependent development of hypertension and alterations in cardiovascular function. *J. Biomech.* **48**, 405–412 (2015).
10. Lee, S., Na, J.-H. & Lee, Y.-M. Epilepsy in Leigh Syndrome With Mitochondrial DNA Mutations. *Front. Neurol.* **10**, (2019).
11. Parker, W. D. & Parks, J. K. Mitochondrial ND5 mutations in idiopathic Parkinson's disease. *Biochem. Biophys. Res. Commun.* **326**, 667–669 (2005).
12. Starikovskaya, E. *et al.* Mitochondrial DNA Variation of Leber's Hereditary Optic Neuropathy in Western Siberia. *Cells* **8**, (2019).
13. Hopkins, J. F. *et al.* Mitochondrial mutations drive prostate cancer aggression. *Nat. Commun.* **8**, (2017).

14. Kalsbeek, A. M. F. *et al.* Mutational load of the mitochondrial genome predicts pathological features and biochemical recurrence in prostate cancer. *Aging* **8**, 2702–2711 (2016).
15. Bacman, S. R. *et al.* MitoTALEN reduces mutant mtDNA load and restores tRNA Ala levels in a mouse model of heteroplasmic mtDNA mutation. *Nat. Med.* **24**, 1696–1700 (2018).
16. He, Y. *et al.* Heteroplasmic mitochondrial DNA mutations in normal and tumour cells. *Nature* **464**, 610–614 (2010).
17. Cui, H. *et al.* Comprehensive next-generation sequence analyses of the entire mitochondrial genome reveal new insights into the molecular diagnosis of mitochondrial DNA disorders. *Genet. Med. Off. J. Am. Coll. Med. Genet.* **15**, 388–394 (2013).
18. Ye, K., Lu, J., Ma, F., Keinan, A. & Gu, Z. Extensive pathogenicity of mitochondrial heteroplasmy in healthy human individuals. *Proc. Natl. Acad. Sci.* **111**, 10654–10659 (2014).
19. Kelly, P. S. *et al.* Ultra-deep next generation mitochondrial genome sequencing reveals widespread heteroplasmy in Chinese hamster ovary cells. *Metab. Eng.* **41**, 11–22 (2017).
20. Hazkani-Covo, E., Zeller, R. M. & Martin, W. Molecular Poltergeists: Mitochondrial DNA Copies (numts) in Sequenced Nuclear Genomes. *PLOS Genet.* **6**, e1000834 (2010).
21. Richly, E. & Leister, D. NUMTs in Sequenced Eukaryotic Genomes. *Mol. Biol. Evol.* **21**, 1081–1084 (2004).

22. Dayama, G., Emery, S. B., Kidd, J. M. & Mills, R. E. The genomic landscape of polymorphic human nuclear mitochondrial insertions. *Nucleic Acids Res.* **42**, 12640–12649 (2014).
23. Goios, A., Carvalho, A. & Amorim, A. Identifying NUMT contamination in mtDNA analyses. *Forensic Sci. Int. Genet. Suppl. Ser.* **2**, 278–280 (2009).
24. Wang, D. *et al.* Mitochondrial DNA enrichment reduced NUMT contamination in porcine NGS analyses. *Brief. Bioinform.* (2019) doi:10.1093/bib/bbz060.
25. Calvignac, S., Konecny, L., Malard, F. & Douady, C. J. Preventing the pollution of mitochondrial datasets with nuclear mitochondrial paralogs (numts). *Mitochondrion* **11**, 246–254 (2011).
26. Goios, A., Prieto, L., Amorim, A. & Pereira, L. Specificity of mtDNA-directed PCR— influence of Nuclear MTDNA insertion (NUMT) contamination in routine samples and techniques. *Int. J. Legal Med.* **122**, 341–345 (2008).
27. Luo, S. *et al.* Biparental Inheritance of Mitochondrial DNA in Humans. *Proc. Natl. Acad. Sci. U. S. A.* **115**, 13039–13044 (2018).
28. Balciuniene, J. & Balciunas, D. A Nuclear mtDNA Concatemer (Mega-NUMT) Could Mimic Paternal Inheritance of Mitochondrial Genome. *Front. Genet.* **10**, (2019).
29. Wei, W. *et al.* Nuclear-mitochondrial DNA segments resemble paternally inherited mitochondrial DNA in humans. *Nat. Commun.* **11**, 1740 (2020).
30. Bai, R. *et al.* Interference of nuclear mitochondrial DNA segments in mitochondrial DNA testing resembles biparental transmission of mitochondrial DNA in humans. *Genet. Med.* 1–8 (2021) doi:10.1038/s41436-021-01166-1.
31. Tamura, K. & Aotsuka, T. Rapid isolation method of animal mitochondrial DNA by the alkaline lysis procedure. *Biochem. Genet.* **26**, 815–819 (1988).

32. Gould, M. P. *et al.* PCR-Free Enrichment of Mitochondrial DNA from Human Blood and Cell Lines for High Quality Next-Generation DNA Sequencing. *PLOS ONE* **10**, e0139253 (2015).
33. Williams, S. L. *et al.* The mtDNA mutation spectrum of the progeroid Polg mutator mouse includes abundant control region multimers. *Cell Metab.* **12**, 675–682 (2010).
34. Avital, G. *et al.* Mitochondrial DNA heteroplasmy in diabetes and normal adults: role of acquired and inherited mutational patterns in twins. *Hum. Mol. Genet.* **21**, 4214–4224 (2012).
35. Hefti, E. & Blanco, J. G. Mitochondrial DNA heteroplasmy in cardiac tissue from individuals with and without coronary artery disease. *Mitochondrial DNA Part DNA Mapp. Seq. Anal.* **29**, 587–593 (2018).
36. Kloss-Brandstätter, A. *et al.* Somatic Mutations throughout the Entire Mitochondrial Genome Are Associated with Elevated PSA Levels in Prostate Cancer Patients. *Am. J. Hum. Genet.* **87**, 802–812 (2010).
37. Li, M., Schröder, R., Ni, S., Madea, B. & Stoneking, M. Extensive tissue-related and allele-related mtDNA heteroplasmy suggests positive selection for somatic mutations. *Proc. Natl. Acad. Sci.* **112**, 2491–2496 (2015).
38. Tranah, G. J., Katzman, S. & Cummings, S. R. MITOCHONDRIAL DNA HETEROPLASMY LEADS TO AGE-RELATED FUNCTIONAL DECLINE AND INCREASED MORTALITY RISK. *Innov. Aging* **1**, 858–859 (2017).
39. Amer, W. *et al.* Evolution analysis of heterogeneous non-small cell lung carcinoma by ultra-deep sequencing of the mitochondrial genome. *Sci. Rep.* **7**, 11069 (2017).

40. Schubert, A. D. *et al.* Somatic mitochondrial mutation discovery using ultra-deep sequencing of the mitochondrial genome reveals spatial tumor heterogeneity in head and neck squamous cell carcinoma. *Cancer Lett.* **471**, 49–60 (2020).
41. Santibanez-Koref, M. *et al.* Assessing mitochondrial heteroplasmy using next generation sequencing: A note of caution. *Mitochondrion* (2018) doi:10.1016/j.mito.2018.08.003.
42. Dai, Y. *et al.* Behavioral and metabolic characterization of heterozygous and homozygous POLG mutator mice. *Mitochondrion* **13**, 282–291 (2013).
43. Perier, C. *et al.* Accumulation of mitochondrial DNA deletions within dopaminergic neurons triggers neuroprotective mechanisms. *Brain J. Neurol.* **136**, 2369–2378 (2013).
44. Safdar, A. *et al.* Endurance exercise rescues progeroid aging and induces systemic mitochondrial rejuvenation in mtDNA mutator mice. *Proc. Natl. Acad. Sci. U. S. A.* **108**, 4135–4140 (2011).
45. Jenuth, J. P., Peterson, A. C. & Shoubridge, E. A. Tissue-specific selection for different mtDNA genotypes in heteroplasmic mice. *Nat. Genet.* **16**, 93–95 (1997).
46. Ma, H. *et al.* Germline and somatic mtDNA mutations in mouse aging. *PLOS ONE* **13**, e0201304 (2018).
47. Liggett, L. A., Sharma, A., De, S. & DeGregori, J. FERMI: A Novel Method for Sensitive Detection of Rare Mutations in Somatic Tissue. *G3 GenesGenomesGenetics* **9**, 2977–2987 (2019).
48. Dai, P. *et al.* Calibration-free NGS quantitation of mutations below 0.01% VAF. *Nat. Commun.* **12**, 6123 (2021).
49. Li, H. Aligning sequence reads, clone sequences and assembly contigs with BWA-MEM. *ArXiv13033997 Q-Bio* (2013).

50. Picard Tools - By Broad Institute. <https://broadinstitute.github.io/picard/>.
51. RStudio, Inc. RStudio: Integrated Development for R.
52. Wickham, H. *ggplot2: Elegant Graphics for Data Analysis*. (Springer-Verlag, 2009).
53. Cingolani, P. *et al.* A program for annotating and predicting the effects of single nucleotide polymorphisms, SnpEff. *Fly (Austin)* **6**, 80–92 (2012).
54. Quiros, P. M., Goyal, A., Jha, P. & Auwerx, J. Analysis of mtDNA/nDNA ratio in mice. *Curr. Protoc. Mouse Biol.* **7**, 47–54 (2017).

REVIEWERS' COMMENTS:

Reviewer #1 (Remarks to the Author):

I appreciate the efforts that the authors have made to revise the method and encourage the acceptance of the manuscript in its current form. Congratulations on the nice contribution.

Reviewer #2 (Remarks to the Author):

In the revised manuscript, Walsh et al. discussed the advantage of their method over Gould et al. They have substantiated their claim regarding the lost coverage in the middle of the mtDNA. Additionally, they have clarified the parts of the manuscripts that were not clear in the first submission.

I firmly believe this manuscript will be of great interest to the readers, and I recommend accepting this work for publication.